Catalysis Communications 109 (2018) 55–59

Contents lists available at ScienceDirect

Catalysis Communications

journal homepage: www.elsevier.com/locate/catcom

Short communication

Constructing interfacial contact for enhanced photocatalytic activity through $BiOIO_3$/g-C_3N_4 nanoflake heterostructure

Jiang Wu[a,*], Pengfei Sheng[a], Weixing Xu[b,*], Xiao Zhou[a], Cheng Lu[a], Zheng Ji[a], Kai Xu[a], Liangjun Zhu[a], Xia Zhang[a], Wei Feng[a]

[a] College of Energy and Mechanical Engineering, Shanghai University of Electric Power, Shanghai 200090, People's Republic of China
[b] Shanghai Huangpu Second Dental Clinic, Shanghai 200021, People's Republic of China

ARTICLE INFO

Keywords:
$BiOIO_3$/g-C_3N_4 heterostructure
Interfacial contact
Nanoflakes
Photocatalyst
Elemental mercury

ABSTRACT

The highly efficient $BiOIO_3$/g-C_3N_4 with unique nanoflake heterostructures were synthesized through hydrothermal method by simply depositing $BiOIO_3$ flake on the surface of g-C_3N_4. Photocatalytic ability of nanoflakes was tested by oxidation of gaseous Hg^0 under 18 W and 24 W LED light irradiation. The g-C_3N_4/$BiOIO_3$ composite with the molar ratio of 10:1 exhibited that the Hg^0 removal efficiency reached up to 93.7%. The remarkable photocatalytic performance of the as-prepared catalysts can be attributed to the interfacial contact heterostructure formed between $BiOIO_3$ and g-C_3N_4, which constructs an intimate interfacial interaction between the two components. Moreover, well-matched band structure can efficiently lead to the separation of photogenerated charges.

1. Introduction

Graphitic-phase carbon nitride (g-C_3N_4), as a metal-free inorganic photocatalyst, has received many researches [1]. In further studies, scientists found that g-C_3N_4 has the characteristics of two-dimensional conjugate structures and can be used as good substrate materials [2,3]. $BiOIO_3$, as a kind of promising bismuth based photocatalyst, has gained much attention nowadays because it is a new noncentrosymmetric and internal polar compound with Aurivillius-type $(Bi_2O_2)^{2+}$ layers, exhibiting many superior properties [4–6]. However, both g-C_3N_4 and $BiOIO_3$ have the same disadvantage, i.e., the recombination of photogenerated charge carriers is too fast [7,8]. The relatively limited absorption under visible-light is another drawback for $BiOIO_3$ [9]. To overcome these shortages, scientists explored many methods such as element doping and co-catalyst modification [10–12]. Recently, formation of heterojunction [13,14] with other semiconductors is considered to be another promising way to improve the performance of g-C_3N_4 by obtaining unique nanostructures and fast charge separation owing to the presence of built-in electric field at the heterostructures interface. Therefore, emphasis has been given on designing novel 2D nanosheet-based heterostructure systems benefiting from 2D structural feature. In particular, due to the notable advantages of the sufficient and tight contact and the improved charge transfer mobility, 2D-2D heterostructures are more than expectation as compared with the 0D-2D and 1D-2D heterostructures [15–18]. Here, we issue a facile strategy for creating 2D layered $BiOIO_3$/g-C_3N_4 heterostructure with intimate interfacial contact via regulating the amount of $BiOIO_3$ deposited on the surface of g-C_3N_4. The built in electric field coupled with $BiOIO_3$/g-C_3N_4 nanoflake heterostructure has been able to achieve such high efficiency. Mercury, a kind of element with high toxicity, strong volatility and persistent durability in bioaccumulation [19], is difficult to be removed by conventional methods because of high oxidation-reduction potentials. The as-prepared 2D-2D heterostructure $BiOIO_3$/g-C_3N_4 nanoflakes are used to oxidizing elemental mercury (Hg^0) to evaluate its photocatalytic performance. Meanwhile, the possible reaction mechanism is elaborated on the basis of characterization and experimental results.

2. Experimental section

2.1. Materials and reagent

Bi $(NO_3)_3{\cdot}5H_2O$, KIO_3 and $C_3H_6N_6$ were obtained from Guoyao Chemical Reagent Co. Ltd. In this study, all chemicals were used as received and all solvents were prepared with ultrapure water.

2.2. Preparation of g-C_3N_4/$BiOIO_3$

Pure g-C_3N_4 powders were obtained by an improved calcination process. Concretely, 10 g of melamine were added to ceramic crucible

* Corresponding author at: No. 2103 Pingliang Road, Shanghai 200090, People's Republic of China.
E-mail address: wjcfd2002@sina.com (J. Wu).

https://doi.org/10.1016/j.catcom.2018.02.018
Received 20 November 2017; Received in revised form 9 February 2018; Accepted 25 February 2018
Available online 26 February 2018
1566-7367/

with a cap, and then maintained at 550 °C for 2 h under the argon atmosphere protection with a heating rate of 5 °C/ min.

In our experiment, 0.1 g g-C_3N_4 was added into 60 mL deionized water, and then ultrasonic treated for 45 min to disperse the g-C_3N_4 completely. After that, an appropriate amount of KIO_3 and a stoichiometric amount of $Bi(NO_3)_3{\cdot}5H_2O$ were dissolved in the suspension and stirred continuously for 45 min. Then, the mixtures were added to a 100 mL Teflon-lined stainless autoclave. All the autoclaves were covered by seals and maintained at 150 °C for 18 h. After reaction, all the autoclaves are placed on the experimental table until they are cooled to room temperature naturally. All the products were filtered and washed by ethanol and ultrapure water for 5 times then dried at 80 °C for 12 h. The g-C_3N_4/$BiOIO_3$ samples with different molar ratios at 10:0.5, 10:0.75, 10:1, 10:2 and 10:4 were prepared according to this method. The as-prepared composites were named as CNB-0.5, CNB-0.75, CNB-1, CNB-2, and CNB-4. $BiOIO_3$ product was also prepared under the same conditions as a reference.

2.3. Photocatalytic activity test

The bench-scale experimental equipment is made up of three main parts, namely simulated on-line mercury analyzer, simulated flue gas (N_2), and photocatalytic reactor, which is consistent with the one we used in our previous studies [20]. Two branches of nitrogen are released from cylinders and controlled by mass flow meters (MFC, CS200) with 0.2 and 1.0 L/min flow rates respectively, one of which with 0.2 L/min passed through mercury generator (PSA, UK) with stated temperature (50 °C). Then, the branch carrying mercury (Hg^0) vapor is mixed with another branch in a mixing tank, then introducing into photocatalytic reactor. The gas-phase Hg^0 concentration is measured by an on-line mercury analyzer (RA-915-M, Lumex, Russia). The catalysts (50 mg) were coated on quartz glass plates (75 mm × 75 mm) by using a dip-coating method, and then it was put into the photocatalytic reactor under 18 W and 24 W LED light (400–450 nm)irradiation, which is shown in Fig. S1. At the beginning of each test, the nitrogen passed through the bypass then was switched to the photocatalytic reactor till the Hg^0 concentration reached the setting value and the on-line mercury analyzer was calibrated. After analyses, the exhaust gas is introduced into the activated carbon and $KMnO_4$ solution bottle to prevent its emission before being expelled into the atmosphere.

The removal efficiency of Hg^0 under 18 W and 24 W LED lamp illumination is calculated using the Eq. (1).

$$\eta_{Hg}(\%) = \frac{Hg_{in}^0 - Hg_{out}^0}{Hg_{in}^0} \times 100\% \quad (1)$$

where $Hg_{in}{}^0$ and $Hg_{out}{}^0$ are Hg^0 concentration (μg/m^3) at the inlet and outlet of the photocatalytic reactor respectively.

3. Results and discussions

3.1. Characterization of $BiOIO_3$/g-C_3N_4 heterostructure

Fig. 1. shows the typical XRD peaks of the g-C_3N_4 sample and $BiOIO_3$/g-C_3N_4 nanosheets with different molar ratio of $BiOIO_3$. Two peaks at 13.04° and 27.47° can be detected in the as-prepared g-C_3N_4, which can be used as the indicators of (100) and (002) crystal face respectively [21]. This result is coincident with the JCPDS card(No. 87-1526). With increasing the amount of $BiOIO_3$, the two peaks decrease in intensity obviously, which indicates that $BiOIO_3$ has been successfully deposited on the g-C_3N_4 surface. The $BiOIO_3$/g-C_3N_4 samples exhibit a two phase constitution: g-C_3N_4 and $BiOIO_3$. All the diffractions of the $BiOIO_3$ sample can be indexed to the orthorhombic phase of $BiOIO_3$ (ICSD #262019). In the composites, the peaks at $2\theta = 27.34°$ can be assigned to the (121) planes of $BiOIO_3$. The (121) diffraction is quite strong, which suggests that the preferential growth was along the (121) direction. The sharp and intense diffraction peaks illustrate that the $BiOIO_3$ has a good degree of crystallinity. It shows that there are no impurities formed between $BiOIO_3$ and g-C_3N_4 because no other phases can be detected in the composites. It is noteworthy that the intensity of characteristic peaks increases first and then decreases with molar doping ratio, and the maximum intensity is at molar ratio 10:1, which is in agreement with the experimental results.

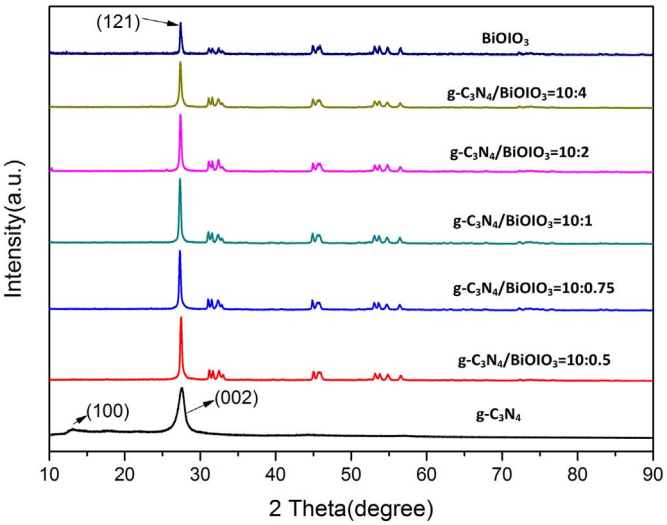

Fig. 1. XRD patterns of the as-prepared g-C_3N_4 and g-C_3N_4/$BiOIO_3$ composites.

The SEM images of g-C_3N_4 and g-C_3N_4/ $BiOIO_3$ composites with diverse molar ratios are demonstrated in Fig.S2. In Fig.S2.a, g-C_3N_4 displays a typically smooth morphology with a lamellar structure. From Fig.S2.b-f, it can be seen clearly that $BiOIO_3$ nanosheets were deposited uniformly on the surface of the g-C_3N_4 after the hydrothermal reaction. When the molar ratio of g-C_3N_4/$BiOIO_3$ is 10:0.5, the sporadic $BiOIO_3$ nanosheets distribute on the surface of g-C_3N_4. When the molar ratio of g-C_3N_4/$BiOIO_3$ reaches to 10:0.75, a thin layer of $BiOIO_3$ nanosheets attach to the g-C_3N_4 surface. The $BiOIO_3$ nanosheets are accumulated and agglomerated on the g-C_3N_4 surface when further increases the amount of $BiOIO_3$ (10:2). When $BiOIO_3$ nanosheets are large in amount (10:4), the g-C_3N_4 is covered by the $BiOIO_3$ nanosheets with high-density. Thus, it could be confirmed that the $BiOIO_3$ effectively distributed on the surface of g-C_3N_4 and formed a large amount of heterostructures with the g-C_3N_4 nanosheets. This result can also be obtained from the XRD and SEM characterization. The specific surface area and porosity of the g-C_3N_4, $BiOIO_3$ and a series of $BiOIO_3$/g-C_3N_4 catalysts were accessed by N_2 absorption–desorption isotherms and BJH pore-size distribution respectively, and the results are shown in Fig.S3 and Table S1. All the as-prepared samples belong to type IV in BDDT classification shape of isotherms with a H_3-type hysteresis loop in the IUPAC classification [22], which indicates the presence of plate slit and mesoporous structure. The results are in good consistent with the SEM patterns.

The TEM and HRTEM images of CNB-1 composite are shown in Fig. 2. In Fig. 2a, it can be obviously seen that the materials are composed of two parts. Fig. 2b shows obvious $BiOIO_3$ lattice fringes corresponding to (121) plane of orthorhombic phase. The one with fringe spaces of 0.282 nm is in accordance with the (002) crystal plane of g-C_3N_4. The above-mentioned lattice fringes are in good agreement with XRD patterns of the samples. Moreover, the close interfacial contact between g-C_3N_4 and $BiOIO_3$ implies the heterostructure is well-formed between them, which are helpful for the migration of charges, thus can improve the photocatalytic efficiency.

The optical properties of as-prepared samples were investigated by the UV–vis diffuse reflectance spectroscopy. In Fig. 3a, the g-C_3N_4 shows the absorption edge is around 530 nm. The pure $BiOIO_3$ scarcely